

---

# Meta Approach to Data Augmentation Optimization

---

Ryuichiro Hataya<sup>1,2</sup>, Jan Zdenek<sup>1</sup>, Kazuki Yoshizoe<sup>2</sup>, Hideki Nakayama<sup>1</sup>  
<sup>1</sup> The University of Tokyo, <sup>2</sup> RIKEN AIP

## Abstract

Data augmentation policies drastically improve the performance of image recognition tasks, especially when the policies are optimized for the target data and tasks. In this paper, we propose to optimize image recognition models and data augmentation policies simultaneously to improve the performance using gradient descent. Unlike prior methods, our approach avoids using proxy tasks or reducing search space, and can directly improve the validation performance. Our method achieves efficient and scalable training by approximating the gradient of policies by implicit gradient with Neumann series approximation. We demonstrate that our approach can improve the performance of various image classification tasks, including ImageNet classification and fine-grained recognition, without using dataset-specific hyperparameter tuning.

## 1 Introduction

Data augmentation is an effective way to improve the performance of CNN models for image recognition tasks, particularly when its policy is optimized for the target dataset. Conventional data augmentation for images consists of image transformation operations, such as random cropping and flipping, and color enhancing including modification of color intensities [20, 27]. However, designing good data augmentation strategies requires profound understanding of the target data and operations. For example, CutOut [11] randomly erases a patch region of each image and is known to improve performance on the CIFAR-10 dataset, but is also reported to degrade the performance on other datasets, e.g., ImageNet [31].

Therefore, automatically designing effective augmentation strategies according to target data and tasks is desirable to improve the performance of image recognition models. One approach to augment existing data is to generate new data samples by interpolating several training images [10, 18, 51] or by using conditional generative models [1, 2]. However, this approach requires a large amount of labeled data [42] and sometimes fails to improve the performance [43], even if powerful conditional generative models are used. On the other hand, some methods improve the performance by efficiently selecting effective combinations of image transformation operations from exponentially large candidate pools [8, 42, 52]. In particular, AutoAugment [8] and its family [6, 9, 17, 21, 29, 30] optimized combinations of operations to improve validation performance and achieved state-of-the-art results.

These methods involve a bi-level optimization: the inner process optimizes parameters of a CNN on training data using a given combination of operations, and the outer process optimizes the combination of operations to maximize the validation performance. Particularly, the inner loop, i.e., training of a CNN, is usually expensive. Therefore, prior works use proxy tasks that adopt small subsets of training datasets or small models [8, 17, 21, 29] or reduce the search space [6, 9, 30] to keep the entire training feasible. Such approaches may result in sub-optimal solutions. We will further review and formalize this problem in Section 2.

In this paper, we tackle the original bi-level optimization problem directly without using proxy tasks or reducing the search space. We propose Meta Approach to Data Augmentation Optimization

---

```

1  cnn.initialize() # parameterized by  $\theta$ 
2  policy.initialize() # parameterized by  $\phi$ 
3  for epoch in range(num_epochs):
4      for train_data, val_data in data_loader:
5          for i in range(num_inner_iters):
6              input = policy(train_data[i]) # augment data by policy
7              criterion = cnn.train(input) # referred to  $f$  in the text
8              cnn.update(criterion)
9              vcriterion = cnn.val(val_data) # referred to  $g$  in the text
10             policy.update(vcriterion)

```

---

Algorithm 1: Our proposed method MADA0 in a Python-like pseudo code. MADA0 optimizes policy as well as cnn by gradient descent with *slight modifications* (highlighted) and *little overhead* to the standard optimization protocol.

(MADA0), which optimizes CNNs and augmentation policies simultaneously by using gradient-based optimization. Here, policies are updated so that they directly increase CNNs’ performance. Naively applying gradient-based optimization to this bi-level optimization requires differentiation through the inner optimization process [15] or computation of the inverse Hessian matrix [3], both of which suffer from large space complexity. These problems are fatal because data augmentation optimization needs to handle large networks, e.g., CNNs for ImageNet. We bypass these issues by using the implicit gradient method with Neumann series approximation. Thanks to these approximations, MADA0 is simple with little overhead as shown in Algorithm 1. Notably, this simplicity allows MADA0 to scale to problems of ImageNet size, which has been nearly impossible for existing bi-level optimization methods [22].

We empirically demonstrate that MADA0 learns effective data augmentation policies and achieves performance comparable or even superior to existing methods on benchmark datasets for image classification: CIFAR-10, CIFAR-100, SVHN and ImageNet, as well as four fine-grained datasets. In addition, we show that MADA0 improves the performance of self-supervised learning on ImageNet. All of the reported results have been achieved *without using dataset-specific configurations*.

## 2 Generalizing Data Augmentation Optimization

In Section 2.1, we describe the preliminaries of data augmentation optimization of AutoAugment family, and then review prior methods by generalizing the problem in Section 2.2.

### 2.1 Designing Data Augmentation Space

Let us define a set of input images  $\mathcal{X}$  and a set of operations  $\mathcal{S}$  consisting of data augmentation operations such as rotation and color inversion. In the AutoAugment family, each image  $x \in \mathcal{X} \subset [0, 1]^D$  is augmented by an operation  $O : \mathcal{X} \rightarrow \mathcal{X}$  with a probability of  $p_O \in [0, 1]$  and a magnitude of  $\mu_O \in [0, 1]$  as illustrated in Figure 1. The magnitude parameter can correspond for example to the degree of rotation, while some operations, such as inversion, have no magnitude parameter. By applying  $K$  consecutive augmentation operations, each image results in  $2^K$  possible images, that is, the number of images virtually increases. This formulation makes the size of the search space  $(|\mathcal{S}| \times [0, 1] \times [0, 1])^K$ , where  $|\mathcal{S}|$  is the size of the operation set.

Operations and accompanied parameters need to be selected so that they minimize the validation criterion, such as the error rate. Usually, this selection is performed heuristically [20, 27]. However, Cubuk et al. showed that data-driven optimization surpasses handcrafted selection [8].

### 2.2 Generalizing AutoAugment Family

Let  $\theta \in \mathbb{R}^M$  denote parameters of a CNN model and  $\phi \in \mathbb{R}^N$  denote parameters of a policy for augmentation, i.e., selection of operations from the operation set and their accompanied parameters  $\{(\mu_O, p_O); O \in \mathcal{S}\}$ . Let the empirical risk be  $f(\theta, \phi; \mathcal{D}_T)$  and the validation criterion be  $g(\theta; \mathcal{D}_V)$ .

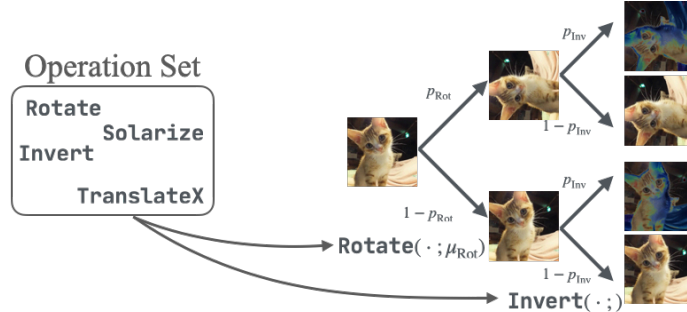


Figure 1: In AutoAugment family, a policy consists of operations. Each operation, e.g., Rotate or Invert, augments an image with a probability of  $p$  and a magnitude of  $\mu$ . As can be seen, performing multiple operations virtually increases the diversity of images. The operations are selected from given operation sets. Our proposed method MADAO learns to select suitable operations and their parameters, and simultaneously optimize a CNN by using gradient descent. This figure shows a 2-stage augmentation.

$\mathcal{D}_T$  and  $\mathcal{D}_V$  are training and validation datasets. In the case of classification task,  $\mathcal{D} := \{(\mathbf{x}_i, y_i)\} \in \mathcal{X} \times \{1, 2, \dots, C\}$ , where  $C$  is the number of classes.

Optimization of data augmentation policy in AutoAugment family methods can be generalized as

$$\operatorname{argmin}_{\phi} g(\operatorname{argmin}_{\theta} f(\theta, \phi; \mathcal{D}_T); \mathcal{D}_V), \quad (1)$$

that is, optimizing CNNs on training data with policies that minimize validation criteria on validation data.

Naïvely solving this bi-level minimization problem takes a long time because CNN training  $\min_{\theta} f(\theta, \phi)$  is costly and the number of possible combinations of augmentation operations and their parameters is infeasibly large. Therefore, prior works tried to alleviate this problem in several ways. One direction is to reduce the search space over augmentation policies, i.e., dimension and range of the parameter  $\phi$  [6, 9, 30]. For example, RandAugment [9] randomly samples operations from the operation set  $\mathcal{S}$  and shares  $\mu_O$  among all operations. This reduction changes the outer problem in Equation (1) from  $\operatorname{argmin}_{\phi} g$  to  $\operatorname{argmin}_{\mu} g$ , which makes it possible to use a simple searching process, such as grid search. OHL-AutoAug [30] enables online searching using policy gradient [49] by restricting the search space only to a limited range.

On the other hand, some methods use proxy tasks that approximate Equation (1) to obtain (sub-) optimal policy  $\phi'$  to reduce the searching time of the inner optimization. The obtained policy  $\phi'$  is then used to train a CNN as  $\min_{\theta} f(\theta, \phi')$  [8, 17, 21, 29] in an “offline” manner. For instance, AutoAugment employs a proxy task  $f'$  that approximates the original inner problem  $f$  as

$$\phi' = \operatorname{argmin}_{\phi} g(\operatorname{argmin}_{\theta'} f'(\theta', \phi'; \mathcal{D}'); \mathcal{D}_V), \quad (2)$$

with a smaller dataset  $|\mathcal{D}'| \ll |\mathcal{D}_T|$  and a smaller network  $\dim \theta' \ll \dim \theta$  for efficiency. The outer problem  $g$  is optimized by black-box optimization techniques, such as reinforcement learning [8]. Fast AutoAugment [29] and Faster AutoAugment [17] approximate Equation (1) as minimizing distance of distributions between augmented images and original images without directly minimizing  $f$ , which allows faster searching.

To summarize, prior methods indirectly solve the bi-level optimization problem in Equation (1), as displayed in Table 1. We instead propose to tackle this problem directly.

### 3 Method

In this paper, we propose to directly optimize the bi-level optimization problem in Equation (1). In other words, we optimize CNNs and augmentation policies *simultaneously*, i.e., in an *online* manner, without reducing the search space or using proxy tasks. With this simultaneous optimization, policies

Table 1: Comparison of prior methods and our proposal, MADAO. **MADAO can efficiently search full space for policies on full datasets with full CNN models**, e.g., on ImageNet with ResNet-50.

Method	Direct Inner Problem	Direct Outer Problem
AutoAugment [8]		✓
Fast AutoAugment [29]		✓
OHL-AutoAug [30]	✓	
RandAugment [9]	✓	
MADAO (ours)	✓	✓

are expected to augment images according to the learning state of CNN models. Algorithm 1 is a simple depiction of our approach, which we call Meta Approach to Data Augmentation Optimization, or in short, MADAO.

### 3.1 Optimizing Policies by Gradient Descent

MADAO directly optimizes the bi-level problem Equation (1) using gradient descent. To this end, we assume that  $f$  and  $g$  are differentiable w.r.t.  $\theta$ . Taking  $C$ -category classification as an example, cross entropy  $-\mathbb{E}_{\mathbf{x}_i, y_i} \log[\mathbf{h}_\theta(\mathbf{x}_i)]_{y_i}$  can be used as  $f$  and  $g$ , but error rate  $\mathbb{E}_{\mathbf{x}_i, y_i} \mathbb{1}(\arg\max \mathbf{h}_\theta(\mathbf{x}_i) \neq y_i)$  cannot. Here,  $\mathbb{1}$  is the indicator function, and  $\mathbf{h}_\theta : \mathbb{R}^D \rightarrow \mathbb{R}^C$  is a CNN with a softmax output layer.

Gradient-based optimization of Equation (1) requires  $\nabla_{\phi} g$  for iterative updating. Since the data augmentation implicitly affects the validation criterion, in other words, data augmentation is not used for validation, we obtain

$$\frac{\partial g}{\partial \phi} = \frac{\partial g}{\partial \theta} \frac{\partial \theta}{\partial \phi}. \quad (3)$$

Because of the requirement of  $g$ ,  $\nabla_{\theta} g$  can be obtained. On the other hand, the exact computation of  $\nabla_{\phi} \theta$  has a large space complexity, as we will describe in Equation (12). Yet, if this gradient was available, the policies could be optimized by gradient descent.

### 3.2 Approximating Gradients of Policy and Inverse Hessian

To obtain  $\nabla_{\phi} \theta$  without suffering from a large space complexity, we can use the Implicit Function Theorem. If there exists a fixed point  $(\theta^*, \phi^*)$  that satisfies  $\nabla_{\theta} f(\theta^*, \phi^*) = 0$ , then there exists a function  $\hat{\theta}$  around  $\phi^*$  such that  $\theta(\phi^*) = \theta^*$ . If this condition holds, we also obtain

$$\frac{\partial \hat{\theta}}{\partial \phi} = - \left( \frac{\partial^2 f}{\partial \theta \partial \theta^\top} \right)^{-1} \frac{\partial^2 f}{\partial \theta \partial \phi^\top} \Big|_{\theta^*, \phi^*}. \quad (4)$$

We can obtain an approximated gradient using this property. Unfortunately,  $M = \dim \theta$  is usually large; therefore, computing the inverse Hessian matrix  $(\nabla_{\theta}^2 f)^{-1}$  is prohibitively expensive as it usually requires  $\mathcal{O}(M^3)$  computations. To avoid computing the inverse Hessian matrix, we use iterative methods based on the Neumann series, which boast better scalability than conjugate gradients in various problems [24, 28, 32].

The Neumann series  $\mathbf{I} + \mathbf{A} + \mathbf{A}^2 + \dots = \sum_i^J \mathbf{A}^i \rightarrow (\mathbf{I} - \mathbf{A})^{-1}$  ( $J \rightarrow \infty$ ) holds with a given squared matrix  $\mathbf{A}$  if  $\|\mathbf{A}\| < 1$ . Using this property, Equation (3) can be approximated with a positive integer  $J$  as

$$\frac{\partial g}{\partial \phi} = - \frac{\partial g}{\partial \theta} \left( \frac{\partial^2 f}{\partial \theta \partial \theta^\top} \right)^{-1} \frac{\partial^2 f}{\partial \theta \partial \phi^\top} \approx - \frac{\partial g}{\partial \theta} \sum_{j=0}^J \left( \mathbf{I} - \frac{\partial^2 f}{\partial \theta \partial \theta^\top} \right)^j \frac{\partial^2 f}{\partial \theta \partial \phi^\top}. \quad (5)$$

We regularize the norm by simply introducing a scalar  $\alpha \in \mathbb{R}^+$  as  $\mathbf{I} - \alpha \nabla_{\theta}^2 f$  as [32]. We use  $\alpha = 10^{-3}$  with  $J = 5$  in the experiments. This Neumann series approximation can also help us avoid explicitly storing the Hessian matrix, whose space complexity is  $\mathcal{O}(M^2)$ , by using Hessian-vector products derived from the following identity:

$$\mathbf{v}^\top \left( \frac{\partial^2 f}{\partial \boldsymbol{\theta} \partial \boldsymbol{\theta}^\top} \right) = \frac{\partial}{\partial \boldsymbol{\theta}} \left( \mathbf{v}^\top \frac{\partial f}{\partial \boldsymbol{\theta}} \right) \quad (\forall \mathbf{v} \in \mathbb{R}^M). \quad (6)$$

This right-hand side can be used instead of storing the Hessian matrix and only has the space complexity of  $\mathcal{O}(2M)$ .

### 3.3 Differentiable Data Augmentation

To differentiate through  $\phi$ , MADAO adopts the differentiable data augmentation pipeline following [17]. As described in Section 2.1, each image  $\mathbf{x}$  is augmented with an operation  $O$  with a magnitude of  $\mu_O$  and a probability of  $p_O$ , which can be written as

$$\mathbf{x} \mapsto \begin{cases} O(\mathbf{x}; \mu_O) & \text{with probability of } p_O \\ \mathbf{x} & \text{with probability of } 1 - p_O. \end{cases} \quad (7)$$

This right-hand side can be written as  $bO(\mathbf{x}; \mu_O) + (1 - b)\mathbf{x}$  with a binary stochastic variable  $b \sim \text{Bern}(b; p_O)$ . Although the original Bernoulli distribution  $\text{Bern}(b; p_O)$  is not differentiable w.r.t.  $p_O$ , Gumbel trick [23] relaxes this restriction to enable backpropagation to update  $p_O$ . Similarly, some color-enhancing operations are non-differentiable w.r.t. the magnitude  $\mu_O$ , so the straight-through estimator [4] is used for such operations. We clamp  $\mu_O$  and  $p_O$  by a sigmoid function to limit their range to  $[0, 1]$ .

MADAO uses a different method to select operations compared to Faster AutoAugment in order to accelerate training. MADAO selects operations using categorical distribution parameterized by a weight parameter  $\boldsymbol{\pi} \in [0, 1]^{|S|}$ , where  $\sum_i \pi_i = 1$ . Since the original categorical distribution is non-differentiable as Bernoulli distribution, we use Gumbel-softmax with a temperature of  $\tau \in \mathbb{R}^+$ . This distribution, referred to as RelaxCat( $\boldsymbol{\pi}; \tau$ ), samples one-hot-like vectors as  $\tau \rightarrow 0$ . Using this distribution, an operation is selected and applied as

$$\mathbf{x} \mapsto \frac{u_i}{\text{SG}(u_i)} O_i(\mathbf{x}; \mu_{O_i}, p_{O_i}), \quad (8)$$

$$i = \text{argmax } \mathbf{u}, \quad (9)$$

$$\mathbf{u} \sim \text{RelaxCat}(\boldsymbol{\pi}; \tau). \quad (10)$$

Here, SG is the stop gradient operation, and thus,  $\frac{u_i}{\text{SG}(u_i)} = 1$  so that the transformation Equation (8) keeps the range in  $(0, 1)$ . Different from this approach, Faster AutoAugment applies all operations and takes the weighted sum of the outputs to approximate this selection.

### 3.4 Connection to Gradient-based Hyperparameter Optimization

As can be seen, Equation (1) is a hyperparameter optimization (HO) problem to neural networks. Traditional HO methods, such as grid search, random search [5] and Bayesian optimization [46], have poor scalability to increasing dimensionality of hyperparameters [22]. For that reason, gradient-based HO attracts attention. From HO viewpoint, policy parameters  $\phi$  are hyperparameters.

As shown in Equation (3), we need to obtain  $\nabla_{\phi} \boldsymbol{\theta}$  to optimize the outer problem  $g$ . The inner optimization process (Algorithm 1 Line 5-8) can be rewritten as

$$\boldsymbol{\theta}_T = \boldsymbol{\theta}_{T-1} - \eta \nabla_{\boldsymbol{\theta}} f(\boldsymbol{\theta}_{T-1}, \phi) = \dots = \boldsymbol{\theta}_0 - \eta \nabla_{\boldsymbol{\theta}} \sum_{t=0}^{T-1} f(\boldsymbol{\theta}_t, \phi) =: \boldsymbol{\theta}_T(\boldsymbol{\theta}_0, \phi) \quad (11)$$

after  $T$  SGD steps with learning rate of  $\eta$ . One approach to obtain  $\nabla_{\phi} \boldsymbol{\theta}$  is to unroll the steps in Equation (11) as [16, 34, 45]:

$$\nabla_{\phi} \boldsymbol{\theta} \approx \nabla_{\phi} \boldsymbol{\theta}_T(\boldsymbol{\theta}_0, \phi). \quad (12)$$

This unrolling requires to cache  $\boldsymbol{\theta}_0, \dots, \boldsymbol{\theta}_{T-1}$ , and thus, the space complexity becomes  $\mathcal{O}(TM)$ , which might be prohibitive for large neural networks, while MADAO requires  $\mathcal{O}(2M)$ .

Alternatively, implicit gradient yields  $\nabla_{\phi}\theta$  as explained in Equation (4). This approach needs the inverse Hessian matrix  $(\nabla_{\theta}^2 f)^{-1}$  [3], but this computation is infeasible for modern neural networks with millions of parameters. Iterative methods, such as conjugate gradient [12, 13, 40, 41] or Neumann series approximation [32], effectively compensate for this issue by approximating this inverse matrix in gradient hyperparameter optimization. Such iterative approximation methods using the Neumann series are also used in approximating influence function [24] and enabling RNNs to handle long sequences [28]. We exploit the knowledge from these prior works and adopt the implicit gradient method with Neumann series approximation to efficiently handle large-scale datasets and CNNs.

## 4 Experiments and Results

This section describes the empirical results of our proposed method in supervised learning for image classification and self-supervised learning tasks. For classification tasks, we use CIFAR-10, CIFAR-100 [26], SVHN [36] and ImageNet (ILSVRC-2012) [44]. In addition, we also used fine-grained classification datasets: Oxford 102 Flowers [37], Oxford-IIT Pets [38], FGVC Aircraft [35] and Stanford Cars [25]. For the self-supervised learning task, we used ImageNet. In all experiments except those on ImageNet, we set 10 % of the original training data aside as validation data  $\mathcal{D}_V$  and report error rates on test data. For ImageNet, we used 1 % of the training data as validation data. Note that this data split means that we use less training data than prior works and that changes the performance of baseline models. More details about experiment configurations are in Appendix B.

We used 14 operations for augmentation: ShearX, ShearY, TranslateX, TranslateY, Rotate, Invert, AutoContrast, Equalize, Solarize, Color, Posterize, Contrast, Brightness and Sharpness (see Appendix A for more details.) To make these operations differentiable, we implemented them using PyTorch [39] and kornia [14]. We scale the magnitude of operations from 0 to 1 so that the magnitude of 0 means no change and the magnitude of 1 corresponds to the strongest level of the particular augmentation operation. We initialized the parameters of magnitude and probability with  $\text{sigmoid}(0.5) \approx 0.62$  and the parameters for operation selection to be equal. That means that MADAO in its initial state is nearly equivalent to RandAugment with the magnitude of 0.62. We set the number of augmentation stages  $K = 2$  in all experiments below (see Figure 1).

For training, we used SGD with a momentum for CNN optimization and RMSprop optimizer with learning rate of  $10^{-2}$  for policy optimization, following [32]. Equation (4) requires the existence of fixed points that satisfies  $\nabla_{\theta} f(\theta, \phi) = 0$ . Following [32], we assume that  $s$  iterations, which corresponds to `num_inner_iters` in Algorithm 1, makes the parameters hold the condition. To further encourage parameters to satisfy the condition, we also used warm up, i.e., training CNNs without augmentation for the first  $w$  epochs. We set  $s = 30$  and  $w = 20$  by default. Validation criterion  $g$  is the same loss function that is used as the training loss function  $f$ , e.g., cross-entropy, for simplicity.

Training of WideResNet 28-2 on CIFAR-10 for 200 epochs with MADAO takes 1.7 hours, while training without MADAO takes 1.0 hours in our environment. As regards memory consumption, training with MADAO requires 3.38 GB of GPU memory, while training without MADAO requires 1.74 GB in this setting. We tune the magnitude parameter of RandAugment using three runs of random search and report the test error rate for the run with the lowest validation error rate.

### CIFAR-10, CIFAR-100 and SVHN

Table 2 presents test error rates on CIFAR-10, CIFAR-100 and SVHN with various CNN models: WideResNet-28-2, WideResNet-40-2, WideResNet-28-10 [50] and ResNet-18 [20]. We show the average scores of three runs. For comparison, we present the results of RandAugment and the default augmentation: Cutout [11], random cropping, and random horizontal flipping (except SVHN), following [9], which we refer to as Baseline. For CIFAR-10 and CIFAR-100, we also present the results of AutoAugment, which are trained on the split training set using the policy provided by the authors<sup>1</sup>. RandAugment and AutoAugment are selected here as representative methods that limit the search space and use proxy tasks, as discussed in section 2.2.

<sup>1</sup><https://github.com/tensorflow/models/tree/master/research/autoaugment>

Table 2: Test error rates on CIFAR-10, CIFAR-100 and SVHN. For AutoAugment\*, we train CNN models with the official AutoAugment policy for CIFAR-10 provided by the authors. **MADAO uses the same hyperparameters for all configurations and achieves superior performance to baselines, which demonstrates the effectiveness of our method.**

Dataset	Model	Baseline	AutoAugment*	RandAugment	MADAO (ours)
CIFAR-10	WideResNet 28-2	4.8	4.7	4.7	4.6
	WideResNet 40-2	4.5	4.3	4.3	4.2
	WideResNet 28-10	3.4	3.1	3.1	3.1
	ResNet-18	5.2	4.5	4.5	4.4
CIFAR-100	WideResNet 28-2	24.8	24.0	24.0	23.9
SVHN	WideResNet 28-2	2.9	N/A	2.6	2.5

Table 3: ImageNet test error rates (Top-1/Top-5) on supervised and self-supervised learning.

Task	Model	Standard	RandAugment	MADAO (ours)
Supervised Learning	ResNet-50	23.7/ 6.9	22.5/ 6.4	23.0/ 6.6
Self-Supervised Learning	ResNet-50	42.1/19.4	39.6/17.6	39.6/17.7

As can be seen, MADAO achieves performance superior to baseline methods, which demonstrates the effectiveness of directly solving the bi-level problem rather than using proxy tasks as AutoAugment or a reduced search space as RandAugment.

### ImageNet

Table 3 shows the results on ImageNet with ResNet-50 [20] trained in supervised and self-supervised learning manners. In the supervised learning setting, we trained models for 180 epochs. In addition, to showcase the effectiveness of MADAO in other tasks than supervised learning, we apply MADAO to contrastive self-supervised learning [19] for 100 epochs of training. We report the results of the linear classification protocol.

Most importantly, MADAO can scale to an ImageNet-size problem without using proxy tasks or reducing search space. We hypothesize that the slightly inferior performance of MADAO compared to RandAugment could be attributed to the fact that ImageNet has 1,000 categories and a single policy might be insufficient for such diverse data. We also believe that class- or instance-conditional data augmentation might be required to further improve performance, which we leave as an open problem.

### Fine-grained Classification

To showcase the ability of MADAO to augment images according to target datasets, we conducted experiments on four fine-grained datasets with ResNet-18 [20]. Table 4 shows the average test error rates over three runs. These datasets are nearly ten to twenty times smaller than CIFARs and SVHN, yet MADAO drastically improves the performance without using dataset-specific hyperparameters. This improvement emphasizes the importance of searching for good policies according to full target datasets from the full search space. MADAO can capture the characteristics of each fine-grained dataset and generate tailored policies for each dataset from a large search space.

Table 4: Test error rates on fine-grained datasets. MADAO outperforms RandAugment with a large margin. **Note that we use the same hyperparameters as in the experiments in Table 2.**

Dataset	Model	# Classes	# Training Set	Standard	RandAugment	MADAO (ours)
Flower	ResNet-18	102	2,040	10.7	8.5	7.5
Pet	ResNet-18	37	3,680	15.0	13.4	12.5
Aircraft	ResNet-18	70	6,667	12.8	9.7	8.7
Car	ResNet-18	196	8,144	14.2	11.3	10.8

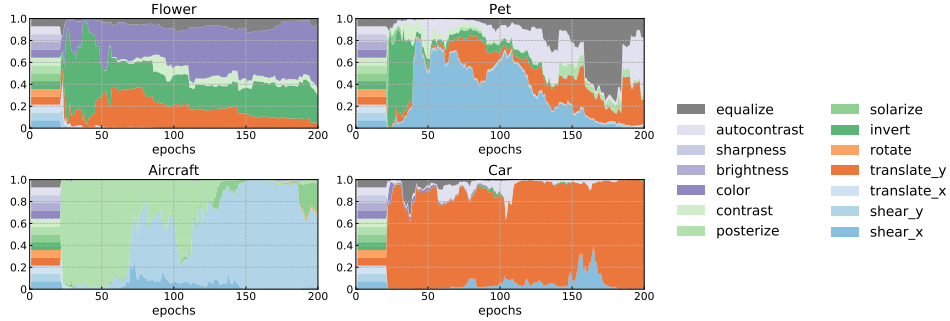


Figure 2: The development of operation selection probabilities at the first augmentation stage during training on fine-grained datasets for 200 epochs. Note that we set the first 20 epochs as a warm-up period during which parameters are not updated.

## 5 Analysis

### 5.1 How Policies Develop during Training

In Figure 2, we present the development of policies during training on fine-grained datasets. As can be seen, each dataset has its specific operations that are selected, which could be thought as reflecting the characteristics of each dataset. Besides, the way of selection changes according to the learning phase. Note that the first 20 epochs are set to warm-up and the augmentation policy parameters are not updated. We show further observations in Appendix C.

### 5.2 How Inner Steps Affect the Performance

Figure 3 presents test error rates with various numbers of inner update steps  $s$  using WideResNet-28-2 on CIFAR-10. CNNs yield the best performance when  $s = 30$  and the results indicate that there exists a trade-off between “exploration and exploitation” of obtained policies: a small number of inner steps might not correctly evaluate the current policies, while running a large number of inner steps might fail to explore better strategies. Importantly, unrolled-based implementations would require to store  $s$  model caches, which is infeasible for  $s = 30$  with modern CNNs. On the other hand, MADAO can efficiently handle a large  $s$ .

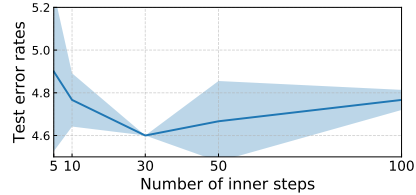


Figure 3: The relationship between the number of inner steps and the final test error rates on CIFAR-10 with WideResNet-28-2. We present the mean and standard deviation over three runs.

## 6 Conclusion

In this paper, we have proposed MADAO, a novel approach to optimize an image recognition model and its data augmentation policy simultaneously. To efficiently achieve this goal, we use the implicit gradient method with Neumann series approximation. As a result, the overhead of MADAO to the standard CNN training, w.r.t., time and memory, is marginal, which enables ImageNet-scale training. Empirically, we demonstrate on various tasks that MADAO achieves superior performance to prior works without restricting search space or using sub-optimal proxy tasks.

Data augmentation is known to boost the performance in various visual representation learning settings, such as semi-supervised learning [6, 47], domain generalization [48], and self-supervised learning [7]. We believe that our method can be introduced into these representation learning methods and efficiently enhance their performance, as we showcased with self-supervised learning in this paper.



## References

- [1] Anthreas Antoniou, Amos Storkey, and Harrison Edwards. “Data Augmentation Generative Adversarial Networks”. In: *ICLR*. 2018.
- [2] Shumeet Baluja and Ian Fischer. “Learning to Attack: Adversarial Transformation Networks”. In: *AAAI*. 2018.
- [3] Yoshua Bengio. “Gradient-based optimization of hyperparameters”. In: *Neural Computation* 12.8 (2000), pp. 1889–1900.
- [4] Yoshua Bengio, Nicholas Léonard, and Aaron Courville. *Estimating or Propagating Gradients Through Stochastic Neurons for Conditional Computation*. arXiv:1308.3432. 2013.
- [5] James Bergstra and Yoshua Bengio. “Random search for hyper-parameter optimization”. In: *JMLR* 13 (2012), pp. 281–305.
- [6] David Berthelot, Nicholas Carlini, Ekin D. Cubuk, Alex Kurakin, Kihyuk Sohn, Han Zhang, and Colin Raffel. “ReMixMatch: Semi-Supervised Learning with Distribution Alignment and Augmentation Anchoring”. In: *ICLR*. 2020.
- [7] Ting Chen, Simon Kornblith, Mohammad Norouzi, and Geoffrey Hinton. *A Simple Framework for Contrastive Learning of Visual Representations*. arXiv:2002.05709. 2020.
- [8] Ekin D. Cubuk, Barret Zoph, Dandelion Mane, Vijay Vasudevan, and Quoc V. Le. “AutoAugment: Learning Augmentation Policies from Data”. In: *CVPR*. 2018.
- [9] Ekin D. Cubuk, Barret Zoph, Jonathon Shlens, and Quoc V. Le. *RandAugment: Practical data augmentation with no separate search*. arXiv:1909.13719. 2019.
- [10] Terrance DeVries and Graham W. Taylor. “Dataset Augmentation in Feature Space”. In: *ICLR*. 2017.
- [11] Terrance DeVries and Graham W. Taylor. *Improved Regularization of Convolutional Neural Networks with Cutout*. arXiv:1708.04552. 2017.
- [12] Chuong B. Do, Chuan Sheng Foo, and Andrew Y. Ng. “Efficient multiple hyperparameter learning for log-linear models”. In: *NIPS*. 2009.
- [13] Justin Domke. “Generic methods for optimization-based modeling”. In: *JMLR* 22 (2012), pp. 318–326.
- [14] D Ponsa E Rublee E. Riba D. Mishkin and G Bradski. “Kornia: an Open Source Differentiable Computer Vision Library for PyTorch”. In: *WACV*. 2019.
- [15] Chelsea Finn, Pieter Abbeel, and Sergey Levine. “Model-Agnostic Meta-Learning for Fast Adaptation of Deep Networks”. In: *ICML*. 2017.
- [16] Luca Franceschi, Paolo Frasconi, Saverio Salzo, and Massimiliano Pontil. “Bilevel Programming for Hyperparameter Optimization and Meta-Learning”. In: *ICML*. 2018.
- [17] Ryuichiro Hataya, Jan Zdenek, Kazuki Yoshizoe, and Hideki Nakayama. *Faster AutoAugment: Learning Augmentation Strategies using Backpropagation*. arXiv:1911.06987. 2019.
- [18] Søren Hauberg, Oren Freifeld, Anders Boesen Lindbo Larsen, John W. Fisher III, and Lars Kai Hansen. “Dreaming More Data: Class-dependent Distributions over Diffeomorphisms for Learned Data Augmentation”. In: *AISTATS*. 2016.
- [19] Kaiming He, Haoqi Fan, Yuxin Wu, Saining Xie, and Ross Girshick. *Momentum Contrast for Unsupervised Visual Representation Learning*. arXiv:1911.05722. 2019.
- [20] Kaiming He, Xiangyu Zhang, Shaoqing Ren, and Jian Sun. “Deep Residual Learning for Image Recognition”. In: *CVPR*. 2016.
- [21] Daniel Ho, Eric Liang, Ion Stoica, Pieter Abbeel, and Xi Chen. “Population Based Augmentation: Efficient Learning of Augmentation Policy Schedules”. In: *ICML*. 2019.
- [22] Frank Hutter, Lars Kotthoff, and Joaquin Vanschoren, eds. *Automatic Machine Learning: Methods, Systems, Challenges*. Springer, 2019.
- [23] Eric Jang, Shixiang Gu, and Ben Poole. “Categorical Reparameterization with Gumbel-Softmax”. In: *ICLR*. 2017.
- [24] Pang Wei Koh and Percy Liang. “Understanding Black-box Predictions via Influence Functions”. In: *ICML*. 2017.
- [25] Jonathan Krause, Michael Stark, Jia Deng, and Li Fei-Fei. “3D Object Representations for Fine-Grained Categorization”. In: *IEEE Workshop on 3D Representation and Recognition*. 2013.

- [26] Alex Krizhevsky. *Learning Multiple Layers of Features from Tiny Images*. Tech. rep. 2009.
- [27] Alex Krizhevsky, Ilya Sutskever, and Geoffrey E Hinton. “ImageNet Classification with Deep Convolutional Neural Networks”. In: *NIPS*. 2012.
- [28] Renjie Liao, Yuwen Xiong, Ethan Fetaya, Lisa Zhang, Ki Jung Yoon, Xaq Pitkow, Raquel Urtasun, and Richard Zemel. “Reviving and improving recurrent back-propagation”. In: *ICML*. 2018.
- [29] Sungbin Lim, Ildoo Kim, Taesup Kim, Chiheon Kim, and Sungwoong Kim. “Fast AutoAugment”. In: *NeurIPS*. 2019.
- [30] Chen Lin, Minghao Guo, Chuming Li, Xin Yuan, Wei Wu, Junjie Yan, Dahua Lin, and Wanli Ouyang. “Online Hyper-Parameter Learning for Auto-Augmentation Strategy”. In: *ICCV*. 2019.
- [31] Raphael Gontijo Lopes, Dong Yin, Ben Poole, Justin Gilmer, and Ekin D. Cubuk. *Improving Robustness Without Sacrificing Accuracy with Patch Gaussian Augmentation*. arXiv:1906.02611. 2019.
- [32] Jonathan Lorraine, Paul Vicol, and David Duvenaud. “Optimizing Millions of Hyperparameters by Implicit Differentiation”. In: *AISTATS*. 2020.
- [33] Ilya Loshchilov and Frank Hutter. “SGDR: Stochastic Gradient Descent with Warm Restarts”. In: *ICLR*. 2016.
- [34] Dougal Maclaurin, David Duvenaud, and Ryan P. Adams. “Gradient-based Hyperparameter Optimization through Reversible Learning”. In: *ICML*. 2015.
- [35] S. Maji, J. Kannala, E. Rahtu, M. Blaschko, and A. Vedaldi. *Fine-Grained Visual Classification of Aircraft*. Tech. rep. 2013.
- [36] Yuval Netzer, Tao Wang, Adam Coates, Alessandro Bissacco, Bo Wu, and Andrew Y. Ng. “Reading Digits in Natural Images with Unsupervised Feature Learning”. In: *NIPS Workshop on Deep Learning and Unsupervised Feature Learning*. 2011.
- [37] Maria-Elena Nilsback and Andrew Zisserman. “Automated Flower Classification over a Large Number of Classes”. In: *Indian Conference on Computer Vision, Graphics and Image Processing*. Dec. 2008.
- [38] Omkar M. Parkhi, Andrea Vedaldi, Andrew Zisserman, and C. V. Jawahar. “Cats and Dogs”. In: *ICPR*. 2012.
- [39] Adam Paszke et al. “PyTorch: An Imperative Style, High-Performance Deep Learning Library”. In: *NeurIPS*. 2019.
- [40] Fabian Pedregosa. “Hyperparameter optimization with approximate gradient”. In: *ICML*. 2016.
- [41] Aravind Rajeswaran, Chelsea Finn, Sham Kakade, and Sergey Levine. “Meta-Learning with Implicit Gradients”. In: *NeurIPS*. 2019.
- [42] Alexander J Ratner, Henry Ehrenberg, Zeshan Hussain, Jared Dunnmon, and Christopher Ré. “Learning to Compose Domain-Specific Transformations for Data Augmentation”. In: *NIPS*. 2017.
- [43] Suman Ravuri and Oriol Vinyals. “Seeing is Not Necessarily Believing: Limitations of BigGANs for Data Augmentation”. In: *ICLR Learning from Limited Labeled Data Workshop*. 2019.
- [44] Olga Russakovsky, Jia Deng, Hao Su, Jonathan Krause, Sanjeev Satheesh, Sean Ma, Zhiheng Huang, Andrej Karpathy, Aditya Khosla, Michael Bernstein, Alexander C. Berg, and Li Fei-Fei. “ImageNet Large Scale Visual Recognition Challenge”. In: *IJCV* (2015).
- [45] Amirreza Shaban, Ching-An Cheng, Nathan Hatch, and Byron Boots. “Truncated Back-propagation for Bilevel Optimization”. In: *AISTATS*. 2019.
- [46] Jasper Snoek, Hugo Larochelle, and Ryan P Adams. “Practical Bayesian Optimization of Machine Learning Algorithms”. In: *NIPS*. 2012.
- [47] Teppei Suzuki and Ikuro Sato. “Adversarial Transformations for Semi-Supervised Learning”. In: *AAAI*. 2020.
- [48] Riccardo Volpi and Vittorio Murino. “Addressing Model Vulnerability to Distributional Shifts over Image Transformation Sets”. In: *ICCV*. 2019.
- [49] Ronald J. Williams. “Simple statistical gradient-following algorithms for connectionist reinforcement learning”. In: *Machine Learning* 8.3-4 (1992), pp. 229–256.
- [50] Sergey Zagoruyko and Nikos Komodakis. “Wide Residual Networks”. In: *BMVC*. 2016.

- [51] Hongyi Zhang, Moustapha Cissé, Yann N. Dauphin, and David Lopez-Paz. “mixup: Beyond Empirical Risk Minimization”. In: *ICLR*. 2018.
- [52] Xinyu Zhang, Qiang Wang, Jian Zhang, and Zhao Zhong. “Adversarial AutoAugment”. In: *ICLR*. 2020.

## A Operations Used in Policies

We introduce the operations used in MADAO in Table 5. Internally, magnitudes are restricted within  $(0, 1)$  range with sigmoid function and rescaled to the appropriate range. For example, we multiply the internal magnitude  $\mu_{\text{ShearX}}$  for ShearX operation by 0.3. As can be seen, there are three operations that have no magnitude parameters. Therefore, each policy has  $(11 + 14 + 14) \times K$  learnable parameters, where 11 corresponds to the number of magnitude parameters, e.g.,  $\mu_{\text{ShearX}}$ , the first 14 corresponds to the number of probability parameters, e.g.,  $p_{\text{ShearX}}$ , and the second 14 corresponds to operation selection parameters  $\pi$ . In our experiments, we set  $K = 2$ , and thus, the total number of learnable parameters is 78. Note that the original implementation of RandAugment does not include Invert in the operation set but we perform experiments with RandAugment using the same operation set as we use for our proposed method, that is including Invert.

Table 5: Operations used in MADAO.

	Operation	Original Magnitude Range
Affine Transformation	ShearX	$[0, 0.3]$
	ShearY	$[0, 0.3]$
	TranslateX	$[0, 0.45]$
	TranslateY	$[0, 0.45]$
	Rotate	$[0, 30]$
Color Enhancing Operations	Invert	none
	AutoContrast	none
	Equalize	none
	Solarize	$[0, 256]$
	Color	$[0, 2]$
	Posterize	$[0, 4]$
	Contrast	$[0, 2]$
	Brightness	$[0, 2]$
Sharpness	$[0, 2]$	

## B Experimental Details

Table 6: Shared hyperparameters in the experiments in Section 4.

Name	Description	Shared Value
Number of inner steps	$s$ corresponds to <code>num_inner_iters</code> in Algorithm 1	30
Warm-up epochs	Initial $w$ th epochs that policy is not updated	20
Temperature	$\tau$ for operation selection	0.05

### B.1 CIFAR-10, CIFAR-100 and SVHN

On CIFAR-10 and CIFAR-100, we trained WideResNets and ResNet-18 for 200 epochs. We used SGD with the initial learning rate of 0.1, the momentum of 0.9 and the weight decay of  $5 \times 10^{-4}$ . The learning rates were scheduled with cosine annealing with warm restart [33]. On SVHN, we trained WideResNet 28-2 for 160 epochs. We used SGD with the initial learning rate of  $5 \times 10^{-3}$ , the momentum of 0.9 and the weight decay of  $1 \times 10^{-4}$ . The learning rate is divided by 10 at 80th and 120th epochs. On CIFAR-10, CIFAR-100 and SVHN, we set the batch size to 128.

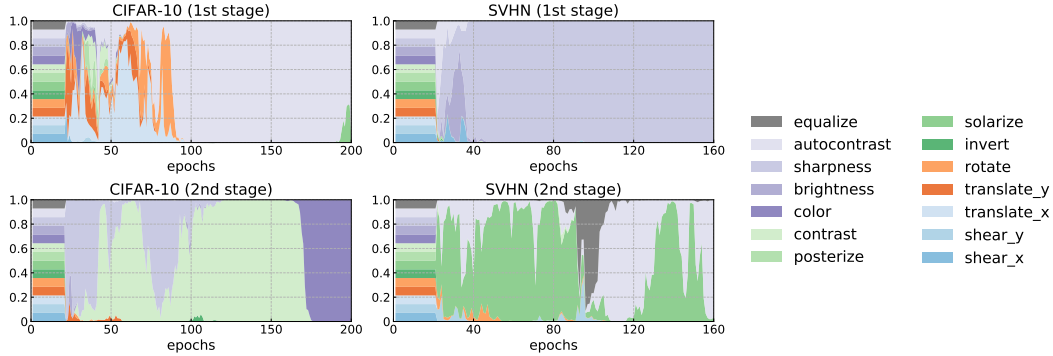


Figure 4: The development of the selection probabilities for each operation during training on CIFAR-10 and SVHN with WideResNet-28-2 for 200 epochs. Note that we set the first 20 epochs to warm-up period that parameters are not updated.

## B.2 ImageNet

### Supervised Learning

On ImageNet, we trained ResNet-50 for 180 epochs with SGD of the base initial learning rate of 0.1, the momentum of 0.9 and the weight decay of  $1 \times 10^{-4}$ . The learning rate is divided by 10 at 60th, 120th and 160th epochs. We set the batch size to 1,024 so that we scale the initial learning rate to 0.4. As the standard data augmentation, we randomly cropped images into  $224 \times 224$  pixels and randomly flipped horizontally.

### Self-supervised Learning

We follow the experimental settings of MoCo [19] and trained for 100 epochs with the batch size of 512 and the queue size of 65,536. We applied augmentation to images for both key and query networks. For linear classification, we used SGD with the momentum of 0.9 and set the initial learning rate to 30, which is decayed by 10 at 60th and 80th epoch.

## B.3 Fine-grained classification

On fine-grained datasets, we trained ResNet-18 for 200 epochs and set the batch size to 64. As the standard data augmentation, we used the same strategy to ImageNet, including random cropping into  $224 \times 224$  pixels.

## C Additional Results

### C.1 How Policies Develop during Training

Figure 4 shows how the selection probabilities for each operation develop during training on CIFAR-10 and SVHN. Similar to fine-grained datasets shown in Figure 2, the policies for CIFAR-10 and SVHN also show clear difference to each other. As can be observed, the first and second stage for each dataset evolve differently, which indicates that the stages develop complementarily to each other.

We also present the development of probability parameters  $p$  and magnitude parameters  $\mu$  in Figure 5. Interestingly, magnitude parameters diverge as training proceeds, while probability parameters remain in the range around the initial value. This observation partially agrees with the way of RandAugment, where RandAugment removes the probability parameter from its hyperparameters. At the same time, this results imply that the optimal magnitudes might be non-global, which disagrees with RandAugment.

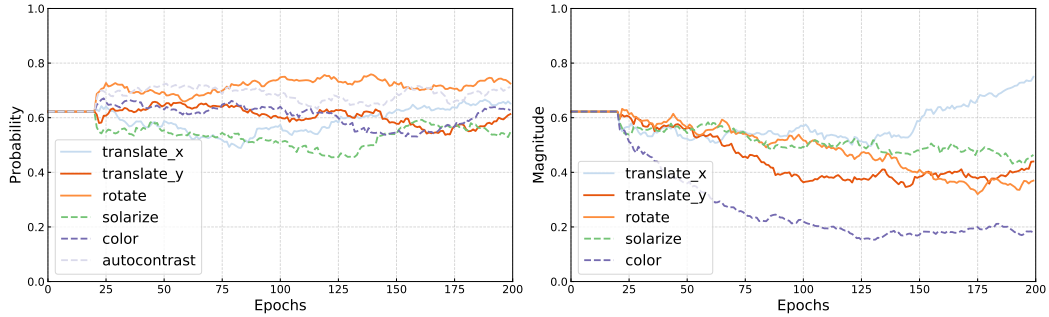


Figure 5: The development of probability parameters  $p$  and magnitude parameters  $\mu$  for often selected operations at the first augmentation stage (corresponds to Figure 4 top left) during training on CIFAR-10 with WideResNet-28-2 for 200 epochs. Note that we set the first 20 epochs to warm-up period that parameters are not updated.

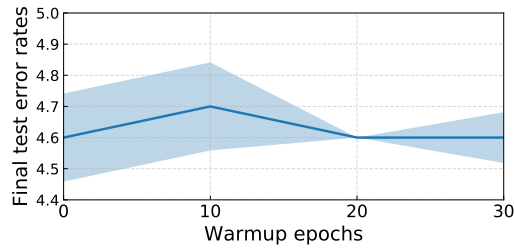


Figure 6: The relationship between the warm-up epochs and the final test error rates on CIFAR-10 with WideResNet-28-2. We present mean and standard deviation over three runs.

## C.2 How Warm-up Affects the Performance

Figure 6 shows the relationship between the warm-up epochs and the final test error rates. There is no significant difference between the selection of warm-up epochs between 0 and 30.

## C.3 Comparison to Policies without Training

On CIFAR-10 with WideResNet-28-2, the initialized policies yield test error rates of 4.7, which is even with RandAugment, as intended. Therefore, policy training yields 0.1 % of performance gain.